Chapter 2

Mid-Infrared Spectroscopy of High-Redshift Submillimeter Galaxies: First Results

We present mid-infrared spectra of five submillimeter galaxies at $z = 0.65-2.38$ taken with the *Spitzer Space Telescope* [1]. Four of these sources, at $z \lesssim 1.5$, have strong features from Polycyclic Aromatic Hydrocarbons (PAHs) and their composite spectrum is well fitted by a starburst-dominated M82-like spectrum with an additional power-law component consistent with that expected from an AGN. Based on comparison with local templates of the 7.7 μm PAH equivalent width and the PAH-to-infrared luminosity ratio, we conclude that these galaxies host both star formation and AGN activity, with star formation dominating the bolometric luminosity. A single source at $z = 2.38$ displays a Mrk 231-type broad emission feature at rest-frame $\sim$8 μm that does not conform to the typical 7.7/8.6 μm PAH complex in starburst galaxies, suggesting a more substantial AGN contribution.

2.1 Introduction

It is over a decade since the discovery of a population of high-redshift galaxies identified through their submillimeter (submm) emission (Smail et al. 1997; Barger, Cowie & Sanders 1999; Eales et al. 1999; Bertoldi et al. 2000; Cowie et al. 2002; Scott et al.

[1] This chapter has been published in similar form as Menéndez-Delmestre et al. 2007.

2002; Borys et al. 2003; Webb et al. 2003a; Coppin et al. 2005; Younger et al. 2007). Their submm selection suggests that these are strongly starbursting systems. With implied star-formation rates (SFRs) of $\sim$ 100–1000 $M_{\odot}\,yr^{-1}$, these dust-enshrouded *submm* galaxies (hereafter, SMGs) may make a significant contribution to the global SFR density at $z \sim 2$–3 (C05). The absorbing dust that makes them such prodigious submm emitters also makes them quite optically faint and renders follow-up studies at shorter wavelengths challenging. The study of SMGs has been facilitated by the detection of a large fraction of them as μJy radio sources (Ivison et al. 2002) and more recently through millimeter-wave interferometry. This has allowed both the reliable identification of their counterparts (Smail et al. 2004), and subsequent measurement of their spectroscopic redshifts for fairly large samples (C05).

With a mean redshift of $<z>\sim 2.2$, the redshift distribution of the *radio-identified* SMGs in C05 coincides with the global peak epoch of quasar activity. The connection between SMGs and AGNs has been probed in recent near-IR and X-ray studies. Near-IR spectroscopy by Swinbank et al. (2004) show that broad Hα lines (FWHM $\gtrsim$ 1000 km s^{-1}) are often present in these galaxies, while deep X-ray studies using the sensitive *Chandra* Deep Field-North (CDF-N) Survey suggest that at least $\sim$28–50% of SMGs host an obscured AGN (Alexander et al. 2005a). A number of SMGs that display no AGN signatures in the rest-frame optical (Swinbank et al. 2004) were classified as AGNs based on X-ray observations (Alexander et al. 2005a). This is likely due to geometrical effects in which the broad-line region of the AGN remains hidden in the optical by intervening obscuring material. At high X-ray energies, direct X-ray emission is detectable through even very high column densities, allowing the direct detection of AGN at very high obscurations. However, Alexander et al. (2005a) find that the majority of AGNs in SMGs are more modestly obscured, with column densities of $N_H \sim 10^{23}$–$10^{24}\,cm^{-2}$. A similar mix of AGN and starburst activity is seen in local ultra-luminous infrared galaxies (ULIRGs; with total infrared luminosities, $L_{8-1000\ \mu m} \gtrsim 10^{12}$; Soifer et al. 1987; Sanders et al. 1988), most of which have been shown to be composite AGN–starburst systems (e.g., Armus et al. 2007). The SMGs have IR luminosities which are comparable to ULIRGs at low redshift,

prompting the question as to whether SMGs are high-redshift analogs of ULIRGs and hence whether we can learn about the physical processes within SMGs from studies of local ULIRGs (Tacconi et al. 2008).

The potential presence of luminous Compton-thick AGNs ($N_H \gtrsim 10^{24}\,cm^{-2}$) in the SMGs with no X-ray AGN signature remains a significant caveat to these results. Furthermore, the samples of SMGs with the necessary ultra-deep X-ray observations to reveal the presence of highly obscured AGN are small. Hence it is possible that a small fraction of luminous, but Compton thick, AGN lurk within the SMG population (see Coppin et al. 2008).

Rest-frame optical emission provides direct insight into the stellar emission and ionized gas of a galaxy, but suffers from obscuration due to intervening dust. At longer wavelengths, the mid-IR emission arising from the dust itself provides an indirect insight into the dust-enshrouded nature of SMGs and suffers from much less obscuration than the shorter, optical wavelengths. We therefore designed a program to follow up a large sample of 24 SMGs in the mid-IR using *Spitzer*'s Infrared Spectrograph (IRS; Houck et al. 2004) in an effort to answer the following questions for a large and representative sample of the SMG population: Are SMGs composite AGN–starburst systems? To what extent does AGN activity contribute to the total infrared output of these galaxies? Is there a spectrum of varying levels of AGN activity across the population? Are local ULIRGs good analogs for the mid-IR emission of SMGs?

The main components contributing to the mid-IR spectrum of a galaxy are: thermal dust continuum, emission from vibrational modes in PAH molecules and other atomic and molecular lines. The continuum emission at longer mid-IR wavelengths, $\lambda \gtrsim 12$ μm, arises from emission by very small grains (VSG; $\lesssim$ 10nm) of dust found around either obscured AGN or in star-forming regions. This is often referred to as the VSG continuum, or the *warm* dust continuum ($T_{Dust} \lesssim 250\,K$). At shorter wavelengths, $\lambda \lesssim 6$ μm, the continuum traces emission from dust heated to significantly hotter temperatures ($T_{Dust} \gtrsim 500\,K$) likely due to its close location near an AGN or possibly a hot, nuclear starburst region. This is what we refer to as the *hot* dust continuum. PAH molecules ($\lesssim$ few nm) consist of chained benzene rings, associated

hydrogen and other trace elements, such as Si and Mg. The line emission in the mid-IR waveband is dominated by PAH molecules which are excited by the UV photons that are copiously available in star-forming regions. The main PAH emission features arise from the bending and stretching of skeletal C-C or peripheral C-H bonds and are observed at rest-frame 6.2, 7.7, 8.6, 11.3, 12.7 and 17 μm (e.g., Draine & Li 2007). The strength of these features have been used in mid-IR surveys with the *Infrared Space Observatory* (ISO; Genzel et al. 1998; Rigopoulou et al. 1999; Tran et al. 2001; Laurent et al. 2000) to estimate the relative contributions of starburst and AGN for the brightest local galaxies (e.g., Rigopoulou et al. 1999). It has been shown locally that stronger PAH features are associated with regions of intense star formation (Helou 1999), while they are typically absent in powerful AGN (Voit 1992).

With the unprecedented sensitivity of *Spitzer* IRS, it has been possible to explore the mid-IR region of galaxies at high redshift down to continuum levels of $S_{24\ \mu m} \gtrsim 0.1$ mJy (e.g., Yan et al. 2005, hereafter Y05; Yan et al. 2007; Lutz et al. 2005, 2007; Desai et al. 2006; Rigopoulou et al. 2006; Teplitz et al. 2007). At lower redshifts, investigation of the mid-IR properties of local galaxies with IRS provide for a sample of detailed templates against which high-redshift sources can be compared (e.g., Spoon et al. 2004; Armus et al. 2004, 2006, 2007; Weedman et al. 2005; Brandl et al. 2006; Sturm et al. 2006; Desai et al. 2007). A wide range of mid-IR spectra has been uncovered for high-redshift sources, ranging from continuum-dominated spectra with no PAH features to PAH-dominated spectra (e.g., Weedman & Houck 2008). Between these two extremes there are a myriad of composite spectra displaying a significant continuum with superposed PAH features (e.g., Yan et al. 2007).

We have an IRS program to study the range of mid-IR properties of a sample of 24 high-redshift SMGs, using the radio-identified sample with spectroscopic redshifts compiled by C05. Here we present IRS spectra of the first five targets observed: four are at lower redshifts, with $z = 0.65 - 1.5$ (SMM J221733.12+001120.2, SMM J163658.78+405728.1, SMM J030227.73+000653.5, SMM J163639.01+405635.9), and one at $z = 2.38$ (SMM J163650.43.43 +405734.5). The spectra of the low-redshift targets cover wavelengths longwards of 10 μm and give insight into the longer mid-

IR emission from SMGs; the full sample is more focused on $z \sim 2$ SMGs and hence probes shorter rest-frame wavelengths (see Chapter 3). This preliminary sample is otherwise representative of the SMG population, in terms of bolometric luminosity, dust temperature and submillimeter-to-radio flux ratio.

2.2 Observations and Reduction

We observed each target using the low resolution Long-Low (LL) observing mode of IRS ($R \sim 57 - 126$) at two different nod positions for 30 cycles of 120s each. We cover rest-frame emission longwards of 6 μm to probe for PAH emission at 6.2, 7.7, 8.6 and 11.3 μm and for silicate absorption centered at 9.7 μm. The data for these first five SMGs were obtained between August 2005 and February 2006.

The data were processed using the Spitzer IRS S13 pipeline [2], which includes saturation flagging, dark subtraction, linearity correction, ramp correction and flat-fielding. With a slit size of $\sim 10.7 \times 168''$, IRS does not resolve the SMGs spatially, and the targets were treated as point sources throughout the data reduction and analysis. We performed additional reduction of the 2D spectra using IRSCLEAN [3] to remove rogue pixels, and relied on differencing between the nod positions to subtract the residual background. We used the SPitzer IRS Custom Extraction (SPICE) [4] software to optimally extract flux-calibrated 1D spectra, by taking a weighted average of profile-normalized flux at each wavelength to increase the S/N of these faint sources. A more detailed description of the observations, reduction and analysis of the entire IRS SMG program is included in Chapter 3.

[2] http://ssc.spitzer.caltech.edu/irs/dh/
[3] http://ssc.spitzer.caltech.edu/archanaly/contributed/irsclean
[4] http://ssc.spitzer.caltech.edu/postbcd/spice.html

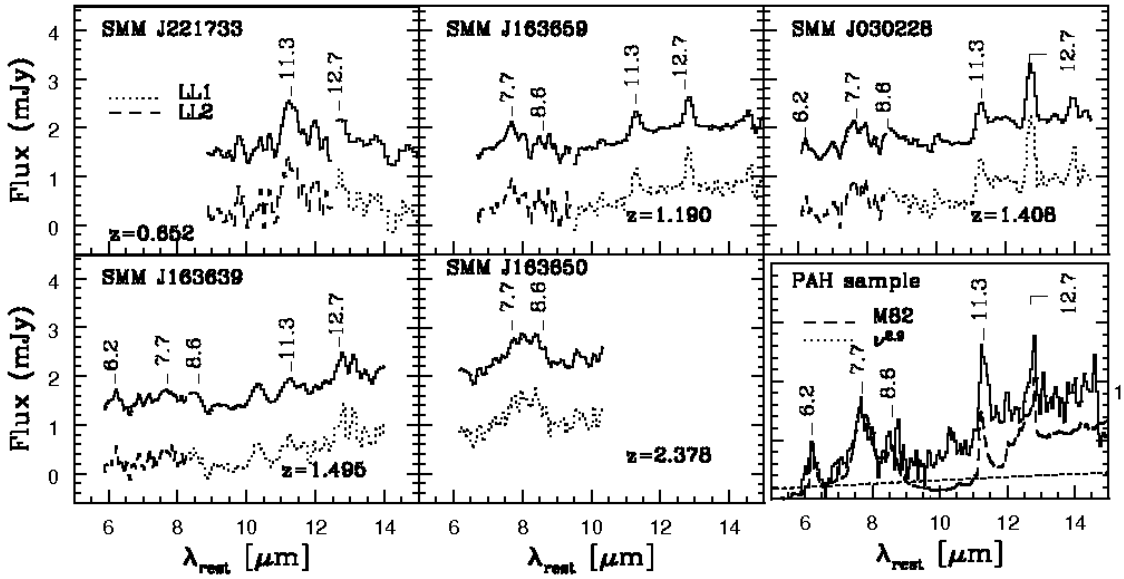

Figure 2.1 Flux-calibrated1D *Spitzer* IRS spectra of five SMGs and the composite spectrum of the PAH sample. For the five individual spectra, the lower curve represents the unsmoothed spectrum, with the first order (LL1: $\lambda_{obs} = 19.5 - 38$ μm) and second order (LL2: $\lambda_{obs} = 14 - 21.3$ μm) of the low-resolution mode shown in dotted and dashed lines, respectively. The upper curve shows the spectrum smoothed by three pixels and offset in flux for clarity. The various wavelengths of PAH emission features are indicated. We show the smoothed version of the composite spectrum for the PAH sample, together with the ISO SWS spectrum of M82 (dashed line), smoothed to the resolution of IRS and normalized to the 7.7 μm PAH feature. The excess in the SMG composite, when fitted by M82, is consistent with an additional power-law component emission from an AGN (dotted line; see §2.3.1.2).

2.3 Results and Discussion

The mid-IR spectra of the SMGs SMM J221733.12, SMM J163658.78, SMM J030227.73 and SMM J163639.01 show moderate to strong PAH features (see Fig. 2.1), and we refer to these targets collectively as the *PAH sample*. Detection of PAH emission is assumed to indicate the presence of starburst activity. At most a very shallow dip is present around 9.7 μm in the spectra, indicating little silicate absorption.

Our highest-redshift source, SMM J163650.43, is somewhat different to the other targets, with a broad emission feature at rest-frame $\sim$8 μm, unlike the typical blended PAH complex of the 7.7 and 8.6 μm features found in starburst galaxies. It is more reminiscent of the spectrum of Mrk 231 (Armus et al. 2007), which features an unabsorbed continuum sandwiched between absorption from silicates at longer wavelengths and from hydrocarbons at shorter ones (Spoon et al. 2004; Weedman et al. 2006). This suggests that SMM J163650.43 has more substantial AGN-activity than the SMGs in the PAH sample, consistent with the presence of a strong CIV (λ1549) feature at rest-frame UV (C05) and a broad Hα component ($\simeq 1753 \pm 238$ km s^{-1}; Swinbank et al. 2004), both revealing the unambiguous presence of an AGN. We discuss the properties of this source in more detail in Chapter 3 (Menéndez-Delmestre et al. 2008) and concentrate here on the median properties of the SMGs with clear PAH emission.

To get an insight into the physics inherent to SMGs in our PAH sample, we compare their spectra with extensively studied local templates: the AGNs Mrk 231 (Armus et al. 2007) and NGC 1068 (Sturm et al. 2000), the starburst M82 (Förster Schreiber et al. 2003) and the more luminous ULIRGs Arp 220 (Armus et al. 2007) and NGC 6240 (Armus et al. 2006). Arp 220 has been a favorite template for high-redshift SMGs (Pope et al. 2006; Kovács et al. 2006): it has strong PAH features, indicative of starburst activity, and a steep mid-IR continuum due to a heavily obscured nuclear component inferred to be responsible for the bulk of the IR luminosity (Spoon et al. 2004). AGNs have been identified in both merging components of NGC 6240 but a starburst dominates the total IR luminosity (Komossa et al. 2003).

A qualitative comparison of the spectra of our PAH sample with these templates rules out Mrk 231, NGC 1068 and Arp 220 as good matches, but the spectra are similar to those of M82 and NGC 6240. Similar results were found by Lutz et al. (2005), who detected strong PAH features in the spectra of two SMGs at $z \sim 2.8$ that were well fitted by an M82-type spectrum.

2.3.1 The Composite SMG Spectrum

We take advantage of the similarity between the spectra in the PAH sample and of our precisely known redshifts (C05) to double our S/N by constructing a composite spectrum by averaging the individual spectra (Fig. 2.1). We use the composite spectrum to make a preliminary assessment of the independent contributions of starburst and AGN activity in our PAH sample. Normalizing the local templates to the 7.7 μm peak in the composite spectrum, we find that the composite is well fitted at $\lambda \lesssim 9$ μm by the NGC 6240 and M82 spectra (Fig. 2.1). However, neither template provides a good fit to the composite spectrum at $\lambda \gtrsim 9$ μm: the continuum emission of NGC 6240 exceeds that of the composite spectrum at $\lambda \gtrsim 12$ μm, while the spectrum of M82 falls below it. No physically reasonable AGN component can be added to the NGC 6240 spectrum to produce a good fit to the composite spectrum at longer wavelengths. On the other hand, an M82-type spectrum plus a power-law continuum provides a good fit to the composite data at all wavelengths.

2.3.1.1 The Starburst Component

The 7.7 μm PAH feature is generally the most prominent in the mid-IR spectra of starburst galaxies. Its strength relative to the continuum, measured by the equivalent width (EW), can be used to evaluate the fractional starburst contribution to the total bolometric output, as the hot mid-IR continuum is enhanced significantly in the presence of an AGN. Starburst-dominated objects, such as M82 and NGC 6240, are characterized by larger PAH EWs than objects with a prominent AGN, such as Mrk 231.

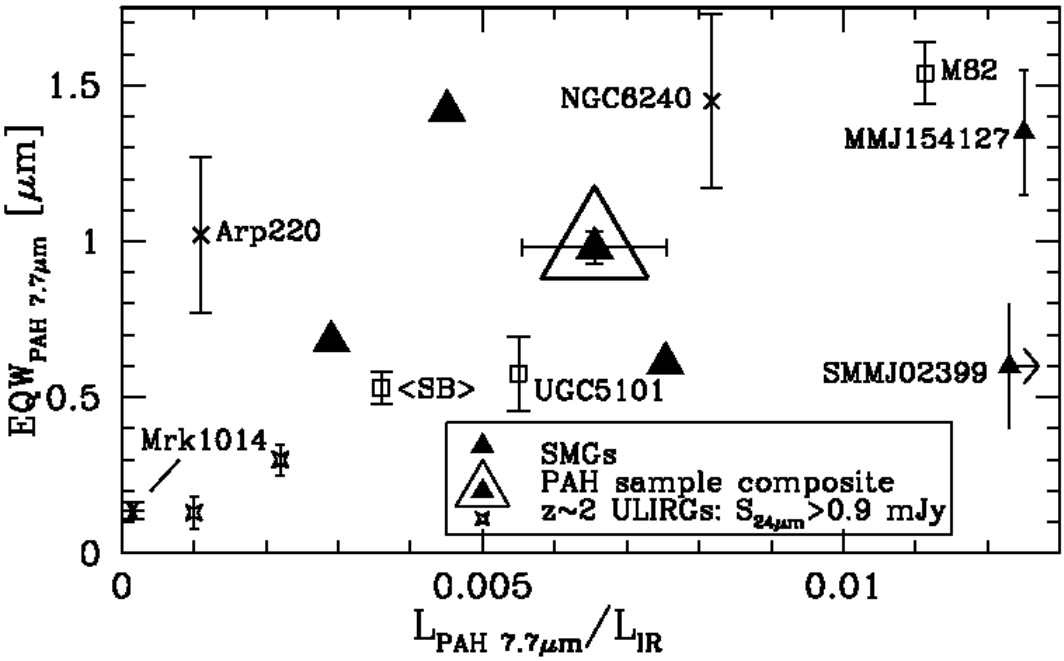

Figure 2.2 Relative strengths of the 7.7 μm PAH feature as measured by the PAH-to-IR ($8 - 1000$ μm) luminosity ratio and the rest-frame EW for the SMGs in the PAH sample (large triangles). We estimate the values for M82 (Förster Schreiber et al. 2003), Arp 220 (Spoon et al. 2004), NGC 6240 (Armus et al. 2006) and for the pair of SMGs in Lutz et al. (2005) (small triangles) directly from their published spectra assuming a linear continuum slope; the error bars reflect the uncertainties of this approach. We derive a lower EW for NGC 6240 than Armus et al. (2006), due to differences in continuum definition. Error bars for the Y05 sources, for the starburst-dominated UGC 5101 (Armus et al. 2004) and for the average of 13 nearby starburst galaxies studied with IRS (Brandl et al. 2006) reflect the uncertainties presented by the authors of the respective papers.

Measured EWs are sensitive to how the continuum is defined. We define a linear continuum by interpolating between two points clear of PAH emission, at 6.8 μm and 13.7 μm, or at 9 μm when the spectrum does not include one or other of these points. In Fig. 2.2 we plot the 7.7 μm rest-frame EWs and PAH-to-IR luminosity ratios for the SMGs in the PAH sample with 7.7 μm coverage and for the composite spectrum. The error in $L_{7.7\ \mu\mathrm{m}}/L_{8-1000\ \mu\mathrm{m}}$ for our SMG sample is dominated by a $\simeq 20\%$ uncertainty in the total IR luminosities (C05) [5]. We compare a number of low- and high-redshift sources, including two ULIRGs at $z \sim 2$ with clear PAH detections from the Y05 sample with $S_{24\ \mu\mathrm{m}} \gtrsim 0.9$ mJy, and two SMGs (SMM J02399−0136 with $S_{850\ \mu\mathrm{m}} = 23$ mJy and MM J154127+6616 with $S_{850\ \mu\mathrm{m}} = 14.6$ mJy) at $z \simeq 2.8$ (Lutz et al. 2005).

According to the line-to-continuum (l/c) diagnostic presented by Genzel et al. (1998), systems with $(l/c)_{7.7\ \mu m} \gtrsim 1$ are classified as starburst-dominated and those with $(l/c)_{7.7\ \mu m} < 1$, as AGN-dominated. With $(l/c)_{7.7\ \mu\mathrm{m}} \gtrsim 1$, starbursts appear to dominate in our PAH sample, that of Y05 and (Lutz et al. 2005). However, the distribution in 7.7 μm EW and PAH-to-IR luminosity ratio in Fig. 2.2 may suggest a distinction in the relative starburst-to-AGN contributions, with lower values of these parameters indicating a stronger AGN contribution. We distinguish three regions in Fig. 2.2: (1) a region with low PAH-to-IR luminosity ratios, occupied by Mrk 1014 (Armus et al. 2004) and the 24 μm-bright sample of Y05; (2) an intermediate PAH-to-IR luminosity region where NGC 6240 and the bulk of the SMGs in our sample are located; and (3) a region with the highest PAH-to-IR luminosity ratios, occupied by M82 and the two SMGs in Lutz et al. (2005).

At $z \sim 2$, the 24 μm flux traces 8 μm rest-frame continuum; a stronger hot mid-IR continuum (produced by an AGN) dilutes the strength of PAH features, leading to lower $L_{7.7\ \mu\mathrm{m}}/L_{8-1000\ \mu\mathrm{m}}$. The location of the Y05 sample in the plot could follow from the selection of 24 μm-bright targets ($S_{24\ \mu m} \gtrsim 0.9$ mJy) at this redshift, which would select objects with lower starburst-to-AGN ratios. SMGs in our sample have higher

[5] Kovács et al. (2006) show that SMGs fall below the local FIR-radio relation and thus the C05-derived $L_{8-1000\ \mu\mathrm{m}}$ values, which rely on this relation, are in average overestimated by a factor of ~ 2.

$L_{7.7\ \mu\mathrm{m}}/L_{8-1000\ \mu\mathrm{m}}$ ratios, similar to NGC 6240, which we interpret as an indication of a markedly stronger starburst contribution to the total luminosity than in the Y05 sample. With similar IR luminosities, the location of the SMG pair from Lutz et al. (2005) in this plot indicates that the 7.7 μm PAH feature is very strong. With large values for both the EW and the PAH-to-IR luminosity ratio, MM J154127 has been suggested to be dominated by starburst activity (Lutz et al. 2005). The large PAH-to-IR luminosity ratio for SMG SMM J02399 suggests strong starburst-activity; however, the relatively low EW value, together with the evident strong mid-IR continuum (see Fig. 2.1, Lutz et al. 2005) is consistent with this source having roughly equal AGN and starburst contributions.

The SMGs in our PAH sample have values of $\mathrm{EW}_{7.7\ \mu\mathrm{m}}$ and $L_{7.7\ \mu\mathrm{m}}/L_{8-1000\ \mu\mathrm{m}}$ that place their starburst-to-AGN ratio between that of the AGN-dominated ULIRG Mrk 1014 and the starburst M82. This is qualitatively similar to NGC 6240, which has both starburst and AGN components. As a caveat, we note that even though the 7.7 μm PAH-to-FIR luminosity ratio is associated with the starburst-to-AGN ratio, it is also sensitive to details of the SED of the system, such as the presence of multiple dust components at different temperatures and the amount of extinction (e.g., Arp 220; Spoon et al. 2004). This may explain the particularly high 7.7 μm PAH-to-IR luminosity ratio for SMM J02399.

2.3.1.2 The AGN Component

Mid-IR line diagnostics suggest that SMGs are starburst-like. The spectra of the starburst-dominated galaxies M82 and NGC 6240 provide a good fit to the composite spectrum at $\lambda \lesssim 9\ \mu$m; however, only an M82-type spectrum with an additional power law AGN component gives a good fit to the composite spectrum at all wavelengths. The power-law component is defined as $S_\nu \sim \nu^{-2.9}$, consistent with the range of IR spectral indices for 3C quasars in Simpson & Rawlings (2000).

From the power-law component flux at 10.5 μm we estimate the X-ray luminosity (L_X) using the correlation between $S_{10.5\ \mu\mathrm{m}}$ and $S_{2-10\mathrm{keV}}$ presented by Krabbe et al. (2001). This yields $L_X \sim 10^{44}\,\mathrm{erg\,s^{-1}}$ for an AGN at the average redshift for the SMGs

presented here, $z \sim 1.4$, in reasonable agreement with the X-ray luminosities found for the SMGs in Alexander et al. (2005a). Following their approach, we compare the average X-ray-to-far-IR ratio of the SMGs in the PAH sample with the typical ratio for quasars and find that the residual flux is consistent with an underlying AGN contributing in the order of $\sim$10% to the total far-IR emission. This agrees with their result that AGN activity is often present in SMGs but does not dominate the energetics. Since the 10.5- μm excess is dominated by lower redshift sources, further SMGs at $z \lesssim 2$, included in Chapter 3 (Menéndez-Delmestre et al. 2008), will better constrain this excess.

2.4 Conclusions

We present first results of a *Spitzer* IRS program to characterize the mid-IR spectra of high redshift SMGs. We compare the spectra to well-studied local templates and find that SMGs have starburst mid-IR spectra more like M82 than the often quoted local analog Arp 220. The composite spectrum of the SMGs in the PAH sample is well fitted by an M82-like starburst-component with a power-law continuum most likely representing a fainter underlying AGN. This similarity to the M82 spectrum suggests that the chemistry of the interstellar medium and radiation fields in these systems may be understood by looking at local galaxies in detail. Analysis of the 7.7 μm equivalent widths and PAH-to-IR luminosity ratios show that SMGs are markedly different from the other 24 μm-selected samples, such as the ULIRGs at $z \sim 2$ (Y05), which have stronger AGN contributions. This work provides further evidence that SMGs host both star formation and AGN activity, but that star formation dominates the bolometric luminosity, reiterating the role of SMGs as the build-up sites for a significant fraction of the stellar content we see today.

An advantage of this sample is that by probing the lower-redshift end of the C05 SMG sample distribution it provides rest-frame wavelength coverage longwards of 9 μm to assess better the AGN contribution. The SMG at $z = 2.38$, with a redshift closer to that of a typical C05 SMG, displays a potentially more AGN-dominated

Mrk 231-type SED, with a broad emission feature at rest-frame ~ 8 μm. The difference in AGN contributions within our preliminary sample suggests an increasing relative AGN-activity in SMGs at higher redshifts, probably due to the 24 μm-based selection of targets. The full sample, with a more extended redshift distribution, will provide us with additional valuable information concerning the typical SMG population.

Acknowledgements We thank the Spitzer Science Center staff for their support, particularly Patrick Ogle for his help in the optimization of the spectral extraction. This work is based on observations made with the Spitzer Space Telescope, which is operated by the Jet Propulsion Laboratory, California Institute of Technology under a contract with NASA. Support for this work was provided by NASA through an award issued by JPL/Caltech.